A forcing mechanism for the poleward flow off the southern California coast

Lie-Yauw Oey

Program in Atmospheric and Oceanic Sciences, Princeton University, Princeton, New Jersey

Abstract. It is shown that when the wind distribution along a coast is anisotropic, such that its cross-shore scale is smaller than its alongshore scale, the coastal sea level (or the upper layer anamoly) "A" of an ocean forced by both wind and wind curl is governed by a modified (nondimensionalized) Kelvin wave equation: $\partial A / \partial t^* + \partial A / \partial y^* = k_0(0, y^*, t^*) + \int \partial k_1 / \partial y^* \, dt_L$ where k_0 and k_1 are wind stress and wind stress curl at the coast, respectively, y is the alongshore distance, and t is the time. Numerical experiments, from a simple reduced-gravity type with idealized forcing and coastline to a three-dimensional primitive equation model with a realistic coastline, bottom topography of the Southern California Bight and the Santa Barbara Channel, and observed wind stresses, were carried out to show that the observed near-coast near-surface poleward flow in the region is primarily forced by the equatorward weakening of the wind curl, $(\partial k_1 / \partial y^* > 0)$, in the bight. Beta provides natural damping by weakening and widening the current through westward propagating Rossby waves and causes the current to lead the coastal pressure field by 1–2 months, which improves the agreement with observations of the phasing of the modeled currents but is otherwise not required in forcing the poleward flow.

1. Introduction

The existence of a near-surface poleward current off the Southern California Bight (SCB; see locator map in Figure 1) has been recognized since *Sverdrup and Fleming* [1941], who referred to it as the Southern California Countercurrent. *Reid et al*. [1958] described the current in terms of a large cyclonic eddy that fills most of the bight. *Schwartzlose* [1963] coined the term "the Southern California Eddy" and used drift bottle data to show its presence during most of the year except spring. This work will focus on the inshore poleward limb of the "eddy." One of the first concrete evidences of the existence of this near-coast near-surface (<50 m) poleward current came from three hydrographic (May, August, and December 1969) and eight drifter-card studies of the Santa Barbara Channel (SBC) oil spill [*Kolpack*, 1971], which, among other things, revealed northeastward (poleward) flow along the eastern and northern coasts of the channel. Farther south, *Hickey*'s [1979] analyses of *Wyllie*'s [1966] (California Cooperative Oceanic Fisheries Investigations (CalCOFI)) data and, in particular, *Tsuchiya*'s [1980] analyses of near-coast hydrographic surveys (1974–1977) between Dana Point (33.5°N) and Del Mar (33°N) both revealed poleward coastal flows especially in late summer through winter. On the basis of the T/S characteristics, Tsuchiya distinguished these from the California Undercurrent, which had its core at ~200–300 m and which was poleward most of the year. Hickey noted that the poleward flow was sometimes continuous with the Davidson Current north of Point Conception (PC), the latter being most intense in winter, and suggested that the two current systems might be dynamically linked. (Recent measurements in the Santa Maria Basin north of PC appear to support Hickey's viewpoint (C. D. Winant, private communication, 1998). These early evidences

of the poleward flow have survived the test of more direct current measurements. *Brink and Muench* [1986] showed measurements (April to June 1983) at the western and eastern ends of the SBC (and on the mainland side of the channel; same below) that indicated poleward flow, especially after mid-May. The 1984 SBC circulation study yielded annual mean currents that were also poleward at both ends of the channel [*Gunn et al*., 1987]. The most recent Minerals Management Service (MMS)-sponsored SBC measurements (1992–1996) [*Harms and Winant*, 1998] showed poleward mean flows year-round, except during spring when the equatorward mean was found near the eastern end of the channel [cf. *Schwartzlose*, 1963; *Tsuchiya*, 1980]. These references to SBC measurements presume that the poleward current is continuous into the channel, which may be problematic because the topography rises to shallower than 300 m in the channel from the deeper main bight's proper in the south, and it is uncertain if the poleward flow is dynamically a near-surface feature (i.e., not merely a surface signature of the poleward undercurrent). On the other hand, direct current-meter measurements exist in the bight, which also clearly indicate poleward mean currents [see *Hickey et al*., 1992, Figure 10].

In summary, there is strong observational evidence that near-surface near-coast poleward current exists in the SCB. The current has speeds of $O(0.1-0.2 \text{ m s}^{-1})$. If dynamically considered as part of the undercurrent, one would presume that the latter somehow intensifies at the surface, which seems difficult to justify. The near-surface near-coast nature of the current suggests a wind-related forcing of some sort and also coastal-trapped dynamics. *Hickey* [1979] recognized the importance of both the wind and wind curl and invoked Sverdrup dynamics to explain the observed poleward flows (similar ideas are taken up by Bray et al., The California Current System in the Southern California Bight and its influence on circulation in the Santa Barbara Channel, manuscript in preparation, 1999)). *Tsuchiya* [1980] reported a seasonal correlation of the
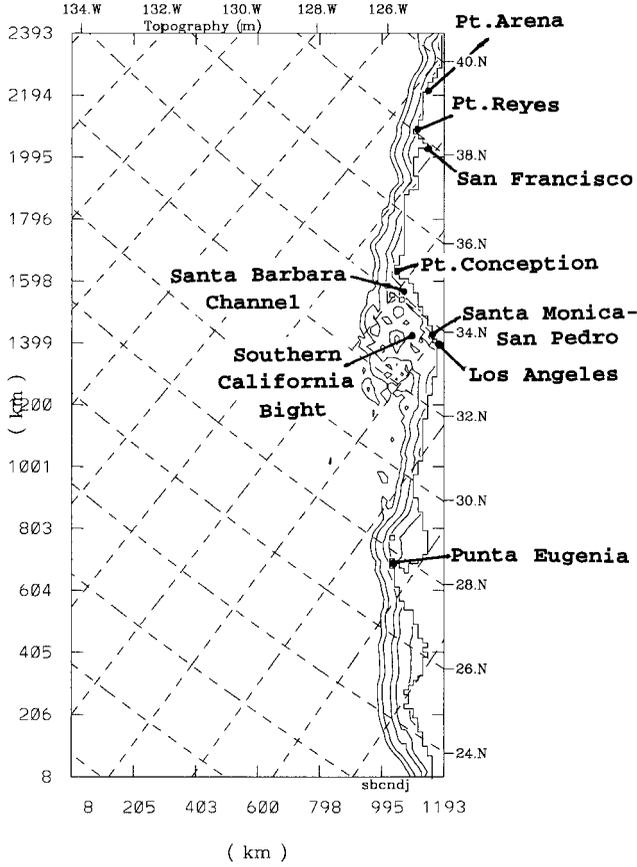
Figure 1. Location map of the continental shelf/slope off California.

current with offshore wind parallel to the coast. *Huyer et al.* [1989] suggested that the current may be driven by alongshore pressure gradients caused by wind relaxation but cautioned that the details were not well understood. This wind-relaxation mechanism is in part supported by *Harms and Winant*'s [1998] analysis of the observations in the SBC.

The objective here is to present a theory of the seasonal variation of the coastal currents off SCB (and SBC). It will be seen that the poleward flow is an integral part of these currents as the wind- and wind curl–driven components compete in a seasonal seasaw. The poleward flow depends on trapped-wave dynamics forced by decrease in the amplitude of the windcurl south of PC and is independent of the mechanism of Sverdrup's β-induced transport. Beta modifies in an important way, however, by weakening and widening the current as well as adjusting phase differences between wind/wind curl, coastal pressure, and currents. Section 2 presents scale analyses based on a 1.5-layer model (the reduced-gravity model), followed in section 3 with calculations that clarify the roles of wind, wind curl, and β. Section 4 extends to calculations with realistic bathymetry (coastline and bottom topography) that are forced by monthly climatological (Comprehensive Ocean-Atmosphere Data Set (COADS)) wind stresses using both the reduced-gravity model and a multilevel, primitive-equation model. Section 5 discusses the model results in light of the observed seasonal variations and small-scale dynamics in the SBC, and section 6 is a summary.

2. Scaling

The ocean is assumed to consist of a thin ($\sim$100–200 m) upper layer of density $\rho_o - \Delta\rho$ overlying an infinitely deep quiescent lower layer of density ρ_o. A meridional coast is placed along the y axis at $x = 0$, so that negative x points to the ocean (i.e., $-\infty < x < 0$). The equations assuming linear dynamics are

$$\partial(\eta)/\partial t + H\nabla \cdot (\mathbf{u}) = 0 \qquad (1a)$$

$$\partial(\mathbf{u})/\partial t + f\mathbf{k} \times \mathbf{u} = -g'\nabla\eta + \tau^o/H \qquad (1b)$$

where $\mathbf{u}$ is the horizontal velocity vector, h is the layer depth, H is a specified undisturbed depth, η is the layer anomaly ($= h - H$), τ^o is the kinematic wind stress, g' is the reduced gravity ($= g\Delta\rho/\rho_o$), $\mathbf{k}$ is the vertical unit vector, t is the time, and f is the constant Coriolis parameter. As will be seen later, the essential dynamics can be elucidated on an f plane.

The customary approach to this wind-forced problem is to assume two length scales [*Gill*, 1982]: an alongshore scale L_y ($\sim$1000 km) coincident with the imposed large-scale wind and a much smaller cross-shore scale of the order of the baroclinic Rossby radius R_o ($\sim$10 km). One finds then, after taking the curl of (1b), that the wind curl part of the forcing is of $O(R_o/L_y)$, which can be safely neglected for timescales of $O(10$ days) or less typical of a passing storm. What this means is simply that the coastal ocean cannot "feel" the gradients of the overlying wind because the latter varies gently offshore and dies off quickly in time. Neither of these is valid off the central and southern California coasts on seasonal timescales. First, the winds are persistently equatorward from spring to fall. Second and more importantly, large wind curl is concentrated in a narrow band of $\sim$100 km offshore [*Hickey*, 1979]. Thus the wind is anisotropic with small cross-shore scale (L_x) and large alongshore scale. The alongshore wind scale can be safely equated to L_y, but treating the cross-shore wind scale the same filters out an important component of the dynamics. To see this, we take the curl of (1b) and make use of (1a) to obtain the (linearized) potential vorticity equation:

$$\partial(\mathrm{PV})/\partial t = \nabla \times \tau^o/H \qquad (2)$$

where $\mathrm{PV} = \zeta - f\eta/H$. Without loss of generality we can assume wind in the alongshore direction only $\tau^o = [0, \tau(x, y, t)]$, so that $\nabla \times \tau^o = \partial(\tau)/\partial x$. Using scalings $x^* = x/R_o$, $y^* = y/L_y$, $t^* = ct/L_y$, $u^* = Hfu/\tau_o$, $v^* = Hcv/(\tau_o L_y)$, and $\eta^* = gH\eta/(\tau_o L_y)$, where $c = (g'H)^{1/2}$, τ_o is the wind scale and the asterisk denotes nondimensional quantities, one obtains:

$$\partial[\partial v^*/\partial x^* - \varepsilon^2 \partial u^*/\partial y^* - \eta^*]/\partial t^*$$
$$= \partial[\tau^*(x^*a, y^*, t^*)]/\partial x^* \qquad (3)$$

where $\varepsilon = (R_o/L_y) \ll 1$ and $a = R_o/L_x$. By explicitly writing x^*a ($=X$, say) as one of the independent variables of τ^*, we recognize that the wind curl may be intense; for otherwise, $L_x = L_y$, $x^*a = x^*\varepsilon$, the right-hand side of (3) $= \partial(\tau^*)/\partial(X) \times \varepsilon = O(\varepsilon)$, and one recovers the constancy of potential vorticity in the customary wind-forced Kelvin wave problem. Integrate (3) in time,

$$\mathrm{PV}^* = \int a\,\partial(\tau^*)/\partial(X)\,dt^* \qquad (4)$$

where $\mathrm{PV}^* = \partial v^*/\partial x^* - \eta^* + O(\varepsilon^2)$, and the ocean is assumed to be initially at rest, $\eta = \mathbf{u} = 0$. Given that $\partial(\tau^*)/$

$\partial(X) \sim O(1)$, there are two physically plausible limits for which PV* is also of $O(1)$. First, the wind varies over a small cross-shore scale of the order of the Rossby radius, $a \sim O(1)$, and over a period $t^* \sim O(1)$ or $t \sim L_y/(R_o f) \sim 5$ to 10 days. This would apply, for example, in the SBC in spring and summer when gusts of intense equatorward wind at the western entrance couple with weak wind inside the channel to produce strong localized curls [Brink et al., 1984]. This limit will be referred to as the localized transient (LT) limit. In the second limit the cross-shore wind scale L_x is larger than R_o (both are $\ll L_y$), $a \sim 0.1$, say, but the wind acts over a long period so that one writes $t_L = at^* \sim O(1)$ in (4). Thus $t \sim L_y/(aR_o f) \sim 50$ to 100 days. This case would correspond to persistent wind curl that acts over the sheltered region just south of PC [Hickey, 1979; Winant and Dorman, 1997]. The spring wind curl map given by Winant and Dorman [1997], for example, suggests a cross-shore scale of ~100 km. This limit will be referred to as the persistent wind curl (PW) limit. In both cases, PV* will be of $O(1)$, and one can expect similar dynamics.

Whereas wind accelerates coastal currents, wind curl does not. Wind curl can drive alongshore flows, however, through alteration of the alongshore pressure field. If windcurl is invariant alongshore, PV* and hence pressure η are also invariant, and one expects zero alongshore flow forced by wind curl (except, of course, the β-induced transport, which is excluded by the present model but which is taken up later). Physically, if positive (negative) wind curl is larger north than south, pressure would be larger (smaller) south than north, and a poleward (equatorward) flow occurs. To see the respective roles of wind and wind curl, the pressure field is examined next.

Take the divergence of (1b) and use (4) to obtain

$$(1 - \partial^2/\partial x^{*2})\eta^* = -\text{PV}^* = -\int \partial(\tau^*)/\partial(X) \, dt_L \quad (5)$$

with an error of $O(\varepsilon^2)$ if the cross-shore component of wind stress is zero and $O(\varepsilon a)$ otherwise. We have also set $t_L = at^*$, which is valid for both the LT (where $a \sim O(1)$) and the PW (where $a \ll 1$ but $at^* \sim O(1)$) limits. The solution to (5) consists of two parts, a part that satisfies the homogeneous form of (5), i.e.,

$$\eta_h^* = A(y^*, t^*) \exp(x^*) \quad (6)$$

and a particular-solution part that is some function of PV*:

$$\eta_p^* = F(\text{PV}^*) \quad (7)$$

which is completely specified once the wind distribution is specified. The problem is closed by specifying the boundary condition at the coast, $u = 0$ at $x = 0$. From (1b), at $x = 0$,

$$v^* = \partial\eta^*/\partial x^* + O(\varepsilon)$$

$$\partial v^*/\partial t^* = -\partial\eta^*/\partial y^* + \tau^*(0, y^*, t^*) \quad (8)$$

(the $O(\varepsilon)$ error vanishes if cross-shore wind equals zero). Eliminate v^* and note that $\eta^* = \eta_h^* + \eta_p^*$ and

$$\partial F/\partial x^* = F' \, \partial\text{PV}^*/\partial x^* = a^2 F' \int \partial^2(\tau^*)/\partial(X^2) \, dt^* \quad (9a)$$

$$\partial F/\partial y^* = F' \partial\text{PV}^*/\partial y^* = F' \int \partial^2(\tau^*)/\partial X \partial y^* \, dt_L \quad (9b)$$

where $F' = d(F)/d(\text{PV}^*)$, we obtain

$$\partial A/\partial t^* + \partial A/\partial y^* = -F' \int \partial^2(\tau^*)/\partial X \partial y^* \, dt_L|_o$$
$$+ \tau^*(0, y^*, t^*) + O(a^2) \quad (10)$$

where $(\quad)|_o$ denotes evaluation at $x = 0$. The $O(a^2)$ term comes from the time derivative of (9a), which is small in the PW limit and in comparison with the time integral in the first term on the right-hand side in the LT limit. Equation (10) is similar to the customary forced Kelvin wave equation except for the time integral term involving gradient of the wind curl along the coast. Note that this additional term survives only in the LT and PW limits, and that not the wind curl but the alongshore gradient of wind curl (and wind, of course) matters in the dynamics.

Expand τ^* in a Taylor's series near the coast:

$$\tau^*(X, y^*, t_L) = k_0(y^*, t_L) + k_1(y^*, t_L)X + O(X^2) \quad (11)$$

where $k_0 = \tau^*|_0$ and $k_1 = \partial\tau^*/\partial X|_0$ are the wind stress and wind stress curl, respectively, at the coast. Substitute (11) into (5) and (7):

$$\eta_p^* = F(\text{PV}^*) = -\text{PV}^*(y^*, t_L) = -\int k_1(y^*, t_L) \, dt_L \quad (12)$$

so that $F' = -1$, $F^{(n)} = 0$, $n > 1$, and (10) becomes

$$\partial A/\partial t^* + \partial A/\partial y^* = \int \partial k_1/\partial y^* \, dt_L + \tau^*(0, y^*, t^*) \quad (13)$$

Equation (13) is the main result of this section. It says that for an equatorward wind ($k_0 = \tau^*(0, y^*, t^*) < 0$) with a curl distribution near the coast that increases poleward ($\partial k_1/\partial y^* > 0$), as in the SBC and SCB, the drivings of the near-shore currents are opposite. The negative coastal wind contributes to a lowering of sea level A, hence an equatorward flow, while the positive alongshore gradient of the wind curl contributes to an increased sea level, hence poleward flow. A specific example of this opposing contribution (for $a \ll 1$) is given by Oey [1996], where it is shown that because of the different timescales with which the two forcings evolve, the k_1 contribution lags the k_0 by ~1 or 2 months. The models of Wang [1997] and Chen [1998] provide the other extreme for $a \sim O(1)$, in which the response occurs in days. Finally, one may also concoct k_0 and k_1 such that the two opposing forcing would result, in the PW limit, in a seasonal seasaw in the SCB and SBC. This and the effects of β will now be addressed.

3. The PW Limit: Seasonal and Beta Effects

Because poleward flow can be produced by beta as well as by the equatorward decrease in the positive wind curl (henceforth referred to as the curl gradient (CG) effect), the two would be difficult to separate from observations and can cause confusion when interpreting model results. To simplify the open boundary specifications, it is a common practice in wind-forced shelf/ slope numerical models to decrease the wind to zero at either or both of the model's cross-shelf open boundaries. If the wind has a nonzero curl and the boundary where the wind is set to zero is "upstream" in the sense of Kelvin-wave propagation, one sees from (13) that such a practice can lead to the generation of an alongshore flow near the coast, which may or may not be realistic. Worse, such alongshore flow may be misinterpreted as being caused by beta. The objective of this section is to describe numerical experiments that clarify the roles of β and CG.

The governing equations are (1a) and (1b), with an additional Newtonian damping term $-\nu\eta$ on the right-hand side of (1a) (for otherwise, the poleward flow component of the solu-
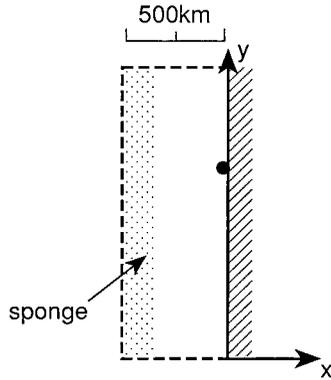
Figure 2. The model domain used for studying effects on coastal poleward flow of meridional gradient of wind curl and β. The solid dot near the coast is where alongshore currents in Figure 3 are plotted.

Figure 3. Alongshore currents (positive poleward) at the coastal solid dot location marked in Figure 2. (a) The 730 day plots for calculations on f plane (solid), on β plane (dash-dotted), f plane with $\partial(\nabla \times \tau^o)/\partial y|_{coast} = 0$ (dotted), and f plane with $\tau^o|_{coast} = 0$ (dashed). (b) Same but for 1460 days and for f plane (solid) and β plane (dash-dotted).

tion grows with time on an f plane). This model will henceforth be referred to as the reduced-gravity (RG) model. Values of parameters are $\beta = 2 \times 10^{-11}$ or 0 m^{-1} s^{-1} centered at 34°N with $f_o = 8 \times 10^{-5}$ s^{-1}, $g' = 2 \times 10^{-2}$ m s^{-2}, $H = 100$ m (thus $R_o \approx 18$ km), and $\nu = 10^{-7}$ s^{-1}. Grid sites are $\Delta x = \Delta y = 5$ km. Experiments with various permutations of these, with $g' = 10^{-2}$ m s^{-2}, $H = 200$ m, $\nu = 10^{-6}$, and 10^{-8} s^{-1} have also been conducted with no change in the conclusions to be discussed below. The model domain is 1500 km alongshore and 500 km cross shore, *Orlanski*'s [1976] radiation at all open boundaries, and an additional 125 km sponge layer near the western boundary to absorb westward propagating Rossby waves when $\beta \neq 0$ (Figure 2; the model ocean is -500 km $< x < 0$ and $0 < y < 1500$ km). Initially, $\mathbf{u} = \eta = 0$, and a seasonally varying southward wind stress is then applied; its form is taken from *McCreary et al.* [1987]:

$$\tau(x, y, t) = \tau_o Y(y)\{[0.5 + 0.4\,Z(t)] + X(x)[0.45$$

$$+ 0.15\,Z(t)]\} \tag{14}$$

where $\tau_o = -10^{-4}$ m^2 s^{-2}, $Y(y) = y/L_y$, where $L_y = 1500$ km, $Z(t) = \cos[\omega(t - 182.5)]$ (t in days), $X(x) = \sin[\pi|x|/(2\Delta)]$ for $-\Delta < x \leq 0$ ($\Delta = 200$ km), and $X(x) = 1$ for $x \leq -\Delta$. Here a linear Y was used instead of the "cosine taper" used by *McCreary et al.* [1987]. The cosine taper will be used later. Thus the wind is weak in the south ($=0$ at the southern boundary) and increases linearly northward. The wind is strongest in summer and weakest in winter; wind curl is positive near the coast and decreases to zero at 200 km from the coast. Four 4 year experiments were conducted with (1) $\beta \neq 0$, (2) $\beta = 0$, (3) $\beta = 0$ and $\partial(\nabla \times \tau^o)/\partial y|_{coast} = 0$, and (4) $\beta = 0$ and $\tau^o|_{coast} = 0$. The results are shown in Figure 3 as plots of the alongshore currents at the coastal location marked in Figure 2 (other locations show similar variations). Experiment 1 shows seasonal equatorward (peak in late spring) and poleward (peak in late fall) flows; the poleward current can be easily misconstrued as being caused by β-induced Sverdrup flow. However, in the absence of β, experiment 2 shows periods of equally energetic equatorward and poleward currents, except that peaks are in summer and winter, respectively. Moreover, in the absence of a meridional gradient of windcurl at the coast (experiment 3), only equatorward current exists, while flow is wholly poleward when wind is zero at the coast (experiment 4). One concludes therefore that the existence of

β is not necessary for the generation of poleward flow in the model and that alongshore gradient of wind curl is responsible for the simulated episodes of poleward flow.

The CG effect is not restricted to the linear $Y(y)$ used in (14). Experiments 1, $\beta \neq 0$, and 2, $\beta = 0$, using the model domain and the form of $Y(y)$ used by *McCreary et al.* [1987] (Figure 4) were repeated. The results are shown in Figure 5 as alongshore currents at the three locations marked in Figure 4 for the (a) $\beta = 0$ case and (b) $\beta \neq 0$ case. The current for the
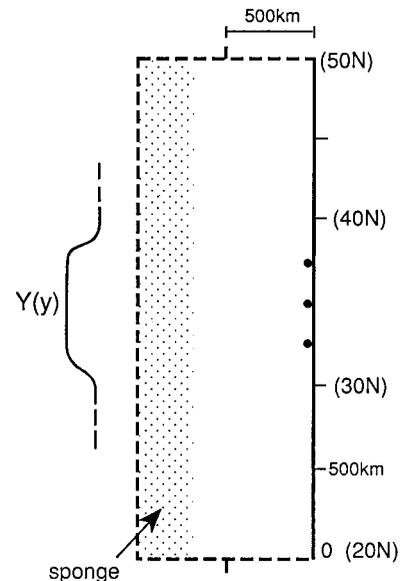
Figure 4. The model domain and the form of $Y(y)$ as used by *McCreary et al.* [1987] for the present reduced-gravity model experiments with $\beta = 0$ and $\beta \neq 0$. The three solid dot locations along the coast are where alongshore currents are plotted in Figure 5.

north location in the $\beta \neq 0$ case is also replotted in Figure 5a for comparison with the corresponding $\beta = 0$ case. For the southern two locations the flows are dominated by poleward flows caused by their proximity to the region of equatorward weakening of the wind and wind curl. These poleward currents exist irrespective of β. At the north location, periods of alternating poleward and equatorward flows exist, again irrespective of β. However, β provides phase shift as well as weakening of the current (the solution with β does not grow with time at zero damping), both caused by westward dispersion of the coastal current through Rossby waves (see below).

4. Models Forced by Monthly Climatological Wind

Does the hypothesis (of poleward flow forced by equatorward weakening of positive wind curl) remain valid under more realistic wind conditions and in a model with coastline and bottom topography? To answer this, two model experiments that use the model domain and bathymetry shown in Figure 1 and that are forced by monthly COADS wind stresses were conducted. The RG model $\Delta x = \Delta y = 5$ km was used in the first experiment, while a three-dimensional (3-D) primitive-equation model was employed in the second experiment.

The RG experiment used COADS wind from 1977 to 1989; it was run with and without the β effect and also with the meridional gradient of COADS wind curl adjusted to zero near the coast (see below). Boundary conditions are identical to those used in the idealized "channel-domain" experiments (Figures 2 or 4). The results are shown in Figure 6 as plots of the alongshore current at PC for two cases: $\beta = 0$ (solid) and $\beta \neq 0$ (dash-dotted). One sees from Figure 6a that periods of poleward flow occur irrespective of β. These occur during fall and winter, while equatorward currents occur during spring. The importance of the alongshore gradient of wind curl is demonstrated in the two experiments shown in Figure 6b. Here the model's y average of COADS winds was used for the first five grid points near the coast (thus the time-dependent wind had curl but was invarient alongshore). The currents are seen
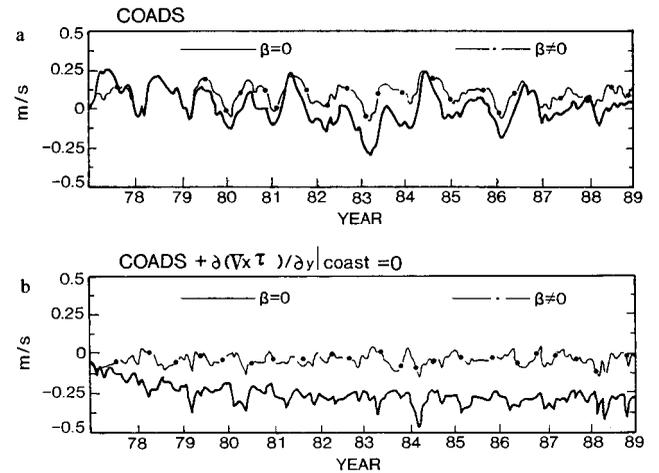
Figure 6. (a) Alongshore currents at Point Conception for the reduced-gravity model experiment with realistic coastline and Comprehensive Ocean-Atmosphere Data Set (COADS) monthly wind stresses (top panel): $\beta = 0$ (solid) and $\beta \neq 0$ (dash-dotted). (b) Same as Figure 6a except that the alongshore gradient of wind curl is zero near the coast (see text).

to be predominantly equatorward. Some periods of poleward flow do occur when $\beta \neq 0$, but these are weak in comparison to the corresponding case shown in Figure 6a when the wind curl weakens equatorward. Thus seasonal poleward flow in the RG model with coastline and under realistic wind conditions prevails as a result of the (observed) alongshore gradient of wind curl irrespective of β.

The 3-D model has 30 equally spaced sigma layers in the vertical and includes realistic bottom topography (Figure 1; see *Oey and Chen* [1992] for a detailed description of the model). It is on the β plane and forced by COADS wind. The model was initialized with a vertical T/S distribution that corresponds to the *Levitus'* [1982] values area averaged over the model domain, and the ocean was at rest. Open boundary conditions are radiation with sponge layer near the western boundary, similar to those used in the RG model experiments [see also *Oey and Chen*, 1992]. In the absence of forcing the model ocean should, and did, remain at rest, as was checked with a 1-year integration without wind. The COADS wind stress was applied (other surface fluxes remained zero) from 1977 to 1983. A quasi-equilibrium state was achieved in ~3 years as checked from kinetic energy plots (not shown). Figure 7 shows the alongshore currents, wind stresses, and wind curl gradient (actually the difference, "north" minus "south," of wind curls between pair of stations) off (a) Punta Eugenia (PE) at 27.8°N, (b) Santa Monica (SM) at 33.8°N, and (c) PC at 34.5°N. All three stations show equatorward flows in spring and summer (April 1980 and 1981, June 1982, and March 1983) when wind stresses become more intensely equatorward (magnitude > 0.7 dyn.cm^{-2}). Poleward flows dominate at other times, and their peaks follow peaks in the alongshore gradient of the wind curl especially for PE and SM, with lags of ~3 months. (Lags of O(months) are consistent with estimates made by *Oey* [1996]). There are also lags on the times of onset of the poleward flows between northern and southern stations: north lags south by ~1 month. This lag is longer than what is expected on the basis of the time taken for a disturbance to propagate at the Kelvin's phase speed along the coast from PE to PC, say, which would

Figure 5. Alongshore currents at the three coastal locations marked in Figure 4: dashed, south location; dotted, middle location; and solid, north location for (a) $\beta = 0$ experiment and (b) $\beta \neq 0$ experiment. For ease of comparison the $\beta \neq 0$ curve at the north location is replotted in Figure 5a as the dash-dotted curve.
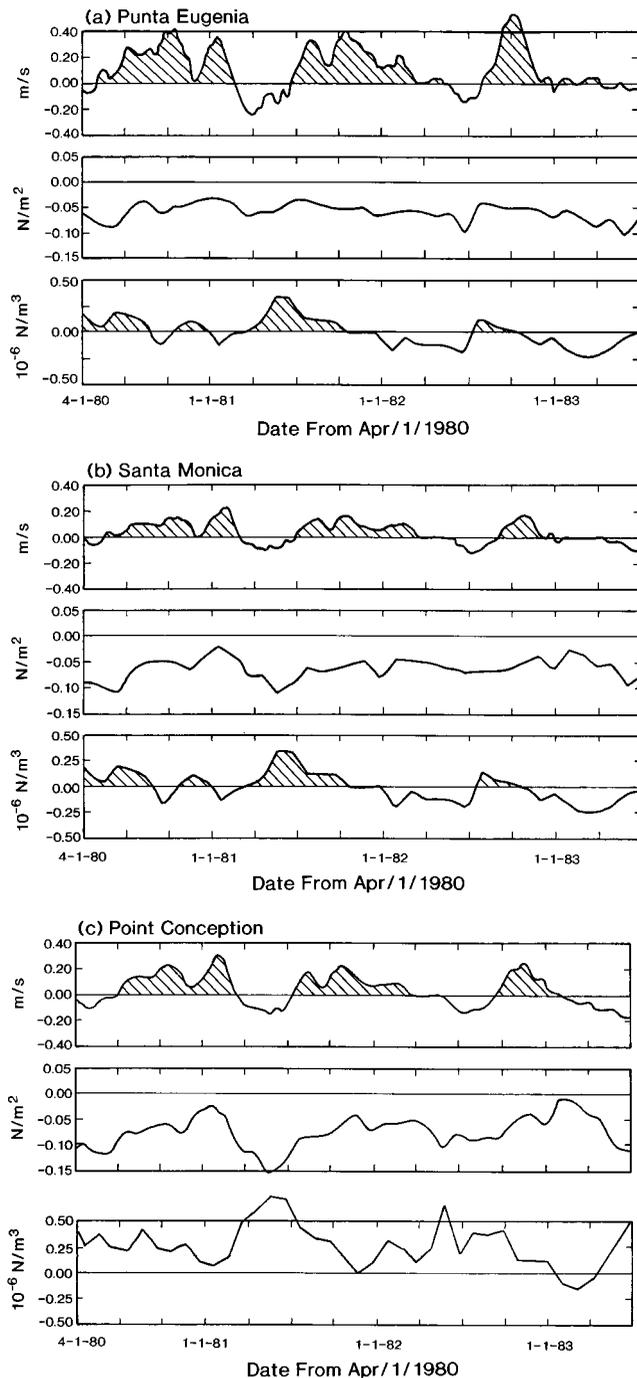
Figure 7. The near-surface alongshore currents from a three-dimensional primitive equation model forced by (top) monthly COADS wind stresses, (middle) wind stresses, and (bottom) wind curl difference between the north and south stations, off (a) Punta Eugenia (PE) at 27.8°N, (b) Santa Monica (SM) at 33.8°N, and (c) Point Conception (PC) at 34.5°N. The wind curl difference off SM in Figure 7b is wind curl at SM minus that at PE, and the plot is repeated in Figure 7a. The wind curl difference off PC in Figure 7c is wind curl at PC minus that at SM. Each tick mark on the time axis is 90 days.

give a lag of ~10–15 days. The reason is because the disturbance is a superposition of two oppositely directed amplitude functions driven by two opposing forcing on the right-hand side of (13). As an extreme example, the alongshore current (say

recorded at a particular coastal station may appear to be unaffected (i.e., remains zero) by forcing due to wind and the alongshore gradient of windcurl to its south because of cancellation, giving an apparent lack of propagation.

The existence in the 3-D experiment of seasonal poleward and equatorward coastal currents that correlate with alongshore gradients of the wind curl (Figure 7) suggests that a discussion of its results in light of the RG-model dynamics will be useful. We will discuss (1) reduction of the 3-D data to a two-layer format, (2) alongshore variability and connection with wind and windcurl, and (3) cross-shelf and temporal variabilities and effects of β.

One way to reduce the 3-D data to a layer format, motivated more by physics than rigorous mathematics, is to define the upper layer as depth (from surface) of an isothermal surface h_T, where T is temperature in degrees Celsius of the isotherm. Three such depths were computed for the 1980–1983 period: h_7, h_9, and h_{11}, corresponding to the 7°C, 9°C, and 11°C isotherms, respectively. We also computed the vertical modal structure based on the simulated density field for 1980 and defined the corresponding upper layer as the depth (h_m) from surface to the point where the first baroclinic-mode eigenfunction changes sign. The h_9 was found to compare particularly well with h_m in terms of both the mean and standard deviation (means and standard deviations for 1980 and averaged over eight grid points (120 km) from the coast are 160 and 98 m for h_m and 170 and 88 m for h_9). The standard deviations for h_7 and h_{11} have similar magnitudes. In the following the 9°C isotherm is chosen to represent the interface that separates upper layer warm water above from lower layer cooler water below. The upper layer depth is $h_U = h_9$, while the lower layer depth is $h_L = D - h_U$, where D is the total water depth (henceforth subscripts U and L will denote upper and lower layer quantities, respectively). Upper (lower) layer currents $\mathbf{V}_U$ ($\mathbf{V}_L$) are defined as averages over h_U (h_L) of the 3-D currents. Friction at the base of the layer (and bottom friction) was also computed; its magnitude was found to be an order smaller than, say, the cross-shore pressure gradient.

Two criteria are used to assess the validity of the RG assumption. First,

$$\text{Bn} = |\mathbf{V}_U|/|\mathbf{V}_L| > 1$$

and preferably $\gg 1$. This criterion implies that $\mathbf{V}_U$ is larger in magnitude than the depth-averaged current $\mathbf{V}_D = (\mathbf{V}_U h_U + \mathbf{V}_L h_L)/(h_U + h_L)$. Since $\mathbf{V}_D \sim 0$ for flow with significant baroclinicity, we will refer to Bn as a baroclinicity index. Second, the depth ratio

$$\text{Hr} = h_L/h_U > 1$$

and preferably $\gg 1$. We also define a stratification index as

$$\text{St} = 2/(h_7 - h_9)$$

in °C m^{-1}, i.e., a function that is inversely proportional to the spacing between the 7° and 9°C isotherms. Since the focus is in the coastal region, these and other field variables were averaged over 120 km cross shore and casted into quantities that were functions of time and alongshore distance y only. The alongshore velocity is V, positive poleward. The averaging distance was based on the width of the poleward surface current, which, because of β, widened to ~100 km (see below; averaging distances of 30 and 60 km were also tested with little change in the results). The functions were then smoothed in
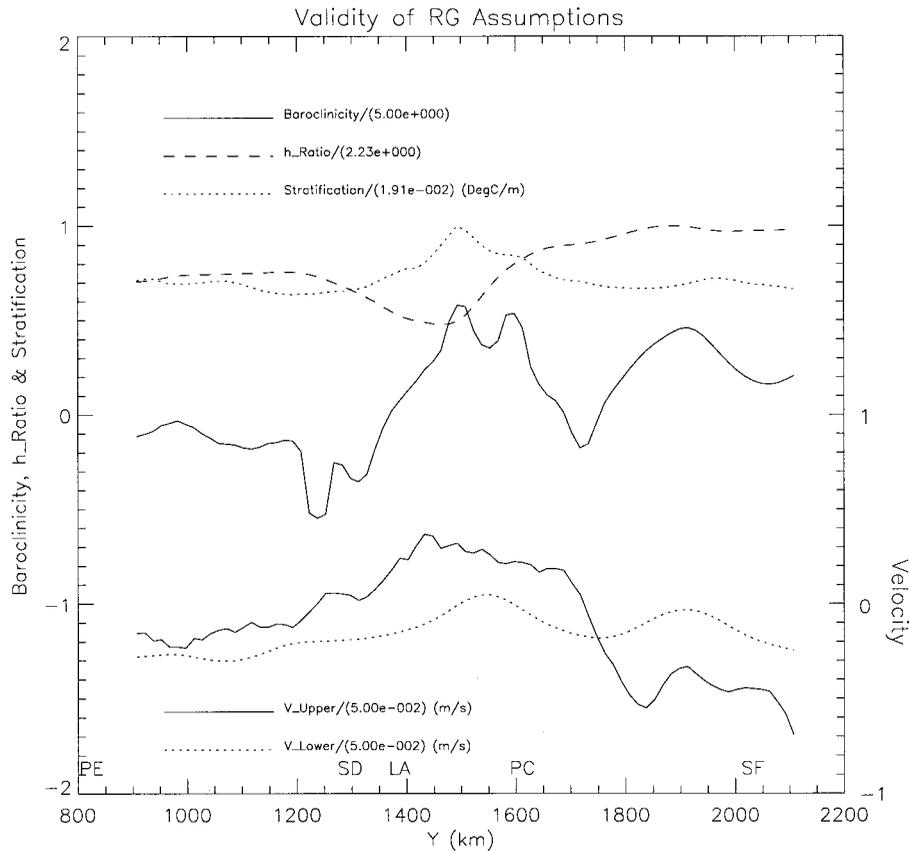
Figure 8. Alongshore variations of the baroclinicity index (Bn) and depth-ratio (Hr) (both expressed as logarithmic), the stratification index (St), and the upper and lower layer alongshore currents (lower two curves). All quantities have been time-averaged from 1980 to 1983 and normalized by values shown in brackets. Regions where ln(Bn) = $-\infty$ were rounded for plotting purpose.

the alongshore direction using a five-point boxcar filter. Figure 8 shows plots of ln($\langle$Bn$\rangle$), ln($\langle$Hr$\rangle$), $\langle$St$\rangle$, $\langle V_U \rangle$, and $\langle V_L \rangle$ from north of PE to San Francisco (SF), where $\langle\ \ \rangle$ denotes time averages from 1980 to 1983. The $\langle$Hr$\rangle$ is everywhere greater than 3 so that the depth-ratio criterion is approximately satisfied. The $\langle$Bn$\rangle$ is >1 north of San Diego (SD; maximum $\sim$ 15 in SBC) except for a narrow region 100 km north of PC where the upper layer current reverses from poleward to equatorward (and must therefore pass through zero). Thus the RG model can be expected to be approximately valid for region north of SD (i.e., a large portion of the SCB) including the SBC. The assumption is particularly good in the SBC (from north of Los Angeles (LA) to PC in Figure 8) where stratification ($\langle$St$\rangle$) also reaches a maximum. On the other hand, although $\langle$Hr$\rangle$ remains large (>4.5) south of SD, $\langle$Bn$\rangle$ drops below, though close to, one (except, again, for a narrow region, just south of SD, where V_U changes sign), which would seem to suggest a breakdown of the RG model. A more detailed examination revealed that the modeled subsurface flow is equatorward for layers below $\sim$200 m, especially over the deep basin ($\sim$60 km offshore). Since h_U thickens to over 200 m south of SD (see below), the subsurface portion of the upper layer contains part of this equatorward flow, while its current near the surface is driven poleward (Figure 7). The V_U, which represents an average over h_U, is therefore weaker than the deeper equatorward flow V_L, thus the apparent breakdown of the RG model. Analysis of the origin and structure of this subsurface equatorward flow, which

is also observed [*Hickey*, 1992], is beyond the scope of this paper.

The approximate validity of the RG assumption suggests that one may check how well the 3-D model response can be interpreted in terms of variations in h_U and V_U as functions of the wind and alongshore gradient of the wind curl. Figure 9 shows the alongshore variations of h_U, V_U, $\partial(\nabla \times \tau^o)/\partial y$, and τ (alongshore wind stress), again time-averaged from 1980 to 1983. The upper layer (h_U) thins from 220 m off Baja to 130 m near San Francisco. Most of the decrease occurs in the region where $\partial(\nabla \times \tau^o)/\partial y$ is positive, from midway between PE and SD to PC. The (positive) $\partial(\nabla \times \tau^o)/\partial y$ is largest between SD to south of PC and weaker in regions south of SD and north of PC (where it reverses sign). In the region of weak $\partial(\nabla \times \tau^o)/\partial y$ south of SD the alongshore flow is equatorward; thus the time-averaged flow is here dominated by the negative τ. (More exactly, the τ and $\partial(\nabla \times \tau^o)/\partial y$ farther to the south should be considered; these remain negative and weak). North of SD, the increasing $\partial(\nabla \times \tau^o)/\partial y$ is followed by a current that reverses poleward (despite equatorward wind), that attains a maximum in the SBC, and that reverses to become equatorward following the maximum of $\nabla \times \tau^o$ at PC (where $\partial(\nabla \times \tau^o)/\partial y = 0$ and <0 farther north). The lagged correlations of the alongshore wind with V_U and also of the alongshore gradient of wind curl with V_U are high ($\sim$0.8) at lags of $\sim$100–200 km. The positive lags mean that the currents lag and are consistent with the RG-model idea that forcing
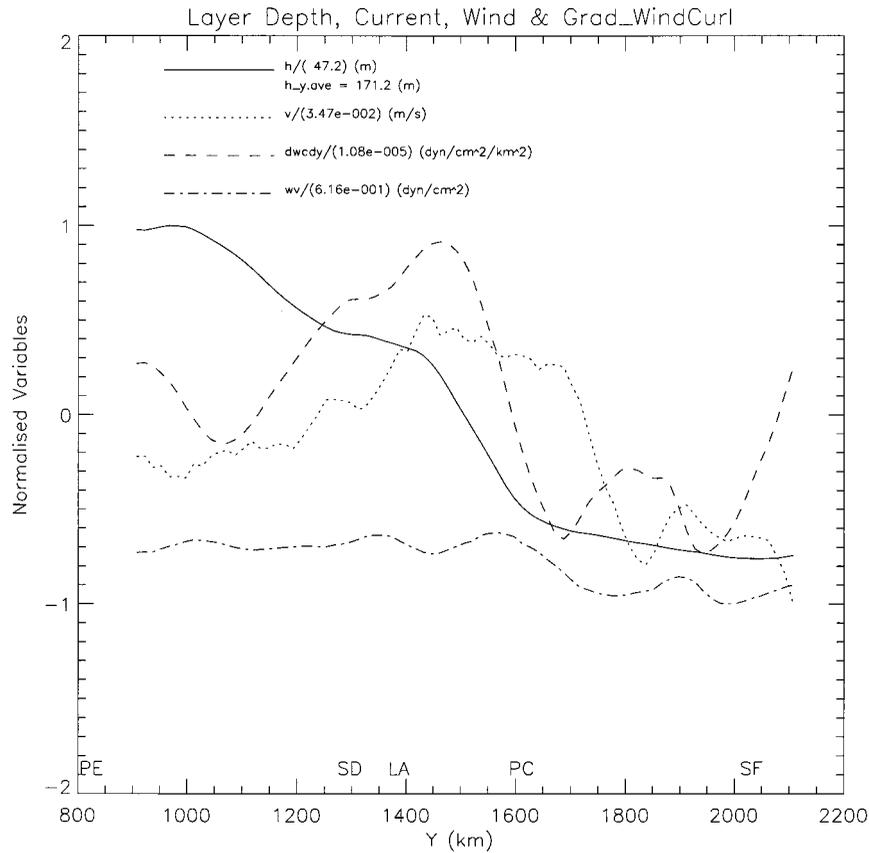
Figure 9. Alongshore variations of the upper layer depth (h_U; solid) and alongshore velocity (V_U; dotted), alongshore gradient of wind curl (dashed), and alongshore wind stress (dash-dotted). All quantities have been time-averaged from 1980 to 1983 and normalized by values shown in brackets. For h_U its alongshore mean (=171 m) was also removed.

originates in the south. The correlation between windcurl and current is small (<0.2) and suggests, as concluded also with the RG-model results, that Sverdrup dynamics are not important in driving the coastal currents.

An example of temporal variabilities is shown in Figure 10 in terms of the cross-shore/time contours of h_U and V_U off PC for the period April 6, 1980 to June 15, 1983. A number of features can be noted. First, the alongshore currents alternate at annual periods between poleward (stippled), from early summer through late winter, and equatorward, from spring through early summer. Second, variation in the upper layer follows closely the current, with a small but significant lag of 55 days (maximum correlation). Thus the upper layer thickens from summer through winter and thins in spring. Except for the lag (the reason for which will be explained shortly) the variations are in accordance with Figure 7 and with the RG-model idea of a combined forcing due to the wind and an alongshore gradient of the windcurl. Finally, disturbances emanate westward from the coast at a speed of ~0.5–1 cm s^{-1}. This may be compared with the first baroclinic Rossby wave phase speed $\sim \beta R_o^2 \sim 0.7$ cm s^{-1} (modal analysis gives a phase speed of ~1.5 m s^{-1} for the first baroclinic mode, so that $R_o \sim 19$ km). Despite the β independence of the basic mechanism that forces poleward and equatorward currents near the coast, Rossby waves spread the coastal influence (Kelvin wave) to ~100 km offshore and in the process weaken currents that would otherwise be trapped within ~20 km of the coast. This β dispersion also explains why

h_U must lag V_U as follows. The alongshore current V_U is very nearly in geostropic balance and in phase with the cross-shore pressure gradient $\partial h_U/\partial x \sim (h_U|_{\text{coast}} - h_U|_{\text{ocean}})/(rR_o)$, where $h_U|_{\text{coast}}$ and $h_U|_{\text{ocean}}$ are layer depths at the coast and at a distance some multiple of the Rossby radius of deformation, rR_o, where $r \sim O(1)$, away from the coast. Suppose $h_U|_{\text{coast}} = e^{iat}$, where $a = 2\pi/P$ and $P = 365$ days. Then $h_U|_{\text{ocean}}$ lags $h_U|_{\text{coast}}$ by the time taken for Rossby wave to propagate cross shelf a distance of rR_o or $h_U|_{\text{ocean}} = e^{ia(t-q)}$, where $q \approx rR_o/(\beta R_o^2) = r/(\beta R_o) \approx 31r$ days. Thus, $h_U|_{\text{coast}} - h_U|_{\text{ocean}} \approx e^{i(at+K)} b|Z|$, where $b = aq \approx 0.53r$, $|Z| = [b^2/4 + (1 - b^2/6)^2]^{1/2}$ and $K = \tan^{-1}(2/b - b/3)$. While the correlation between $(h_U|_{\text{coast}} - h_U|_{\text{ocean}})$ and V_U is significant (>0.7) within 100 km of the coast, a maximum (=0.83) was found at $r = 2$, for which $|Z| \approx 1$ and $K \approx \pi/3$. Thus $\partial h_U/\partial x$, hence V_U, leads h_U by $KP/(2\pi) \approx 60$ days (the actual lag is 55 days in Figure 10).

This explanation of why V_U must lead h_U on the β plane also clarifies the role of β in Figure 5a. Currents on the f plane (solid curve) peak in summer (winter), while those on the β plane (dash-dotted curve) peak 1–2 months earlier in more accordance with observations [e.g., *Hickey*, 1979]. Kelvin wave dynamics are valid in both cases near the coast. On the f plane, cross-shelf pressure differences, hence currents, are in phase with the near-coast pressure field. Thus the solid curve indicates also the coastal pressure variation in both the f and β planes, which must lag the current on the β plane.

a HT (m)

CMIN= 1. CMAX= 500.
CI= 25.

b VT (m s^{-1})

CMIN= −0.5 CMAX= 0.5
CI= 0.05

TREF=9C. 4. 6.1980− 6.15.1983

TREF=9C. 4. 6.1980− 6.15.1983
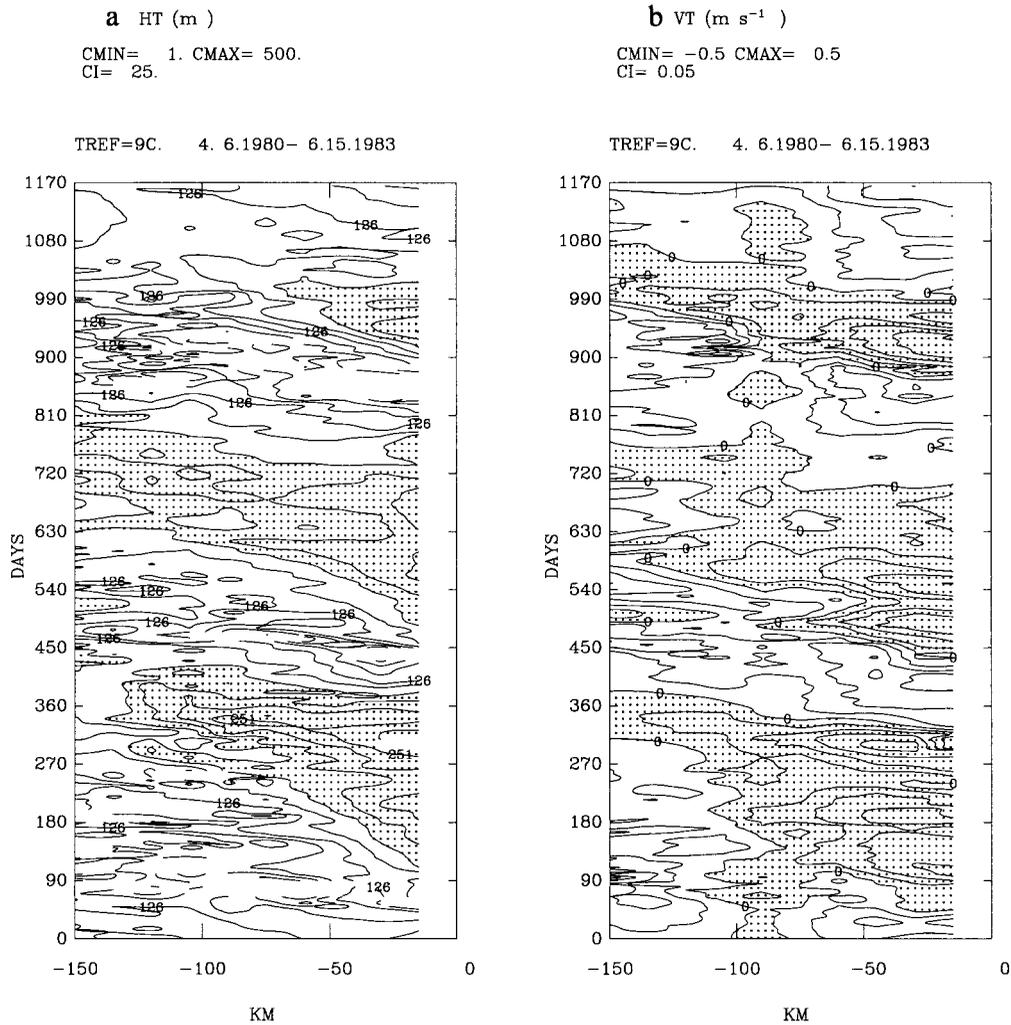
Figure 10. (a) Cross-shore/time contours of the upper layer depth (h_U; contour interval is 25 m, shaded > 176 m) and (b) alongshore velocity (V_U; contour interval is 0.05 m s^{-1}, shaded > 0 or poleward) at Point Conception. The time axis begins April 6, 1980, and ends June 15, 1983; each tick mark is 90 days.

5. Discussion

In addition to *Hickey*'s [1992] direct current observations in the Santa Monica-San Pedro Basin (33°20′–34°N) that show persistent poleward currents in the SCB near-shore region (except perhaps during spring), there also exists, from 1992 to 1994, a comprehensive observational study north of Hickey's site in the SBC. This study was led by Clinton Winant of the Scripps Institute of Oceanography, sponsored by the Mineral Management Service, and included, among other quantities, measurements of the winds, currents, temperature, salinity, and drifter trajectories. The study has led to a better understanding of the current variabilities in the channel, both in the short (O (days)) and seasonal (O (months)) timescales, as summarized in several publications and manuscripts. Of immediate relevance in this discussion are those of *Winant and Dorman* [1997], *Harms and Winant* [1998], and *Harms* [1996]. These and Hickey's work piece together a picture of the regional circulation dynamics that is not inconsistent with the theory presented herein.

A schematic of the seasonal circulation is proposed in Figure 11. In spring the wind (its means are assumed equatorward in all seasons) off PC (western end of SBC) and off the coast of

the SCB and farther south begins to intensify. The latter would produce, through Kelvin wave dynamics, an equatorward current along the coast: in the SCB, the SBC, and around PC to the north. This along-coast flow would result in the accumulation of cyclonic vorticity at the coastline bend near PC, which would then be advected into the channel and lead to the formation of a cyclone in the western part of the channel (eddy-shedding mechanism) [*Oey*, 1996]. There are at least two other mechanisms by means of which cyclone may be formed. The first is due to Ekman divergence in a localized region over which the positive wind curl acts, which according to (3) would lead to raised isopycnal ($\eta < 0$; as well as cyclonic vorticity) and hence cyclonic eddy via geostrophy. This mechanism does not depend on the existence of the coast (or the channel for that matter). However, since observations indicate near-coast intensification of the northern and southern limbs of the cyclone, the mechanism does assume that the localized positive wind curl fills the width of the western portion of the channel, a condition that may not be supported by the observed wind distribution. Recent data (C. E. Dorman, private communication, 1998) indicate that wind off PC turns in the east/ southeastward direction into the channel, most intense near
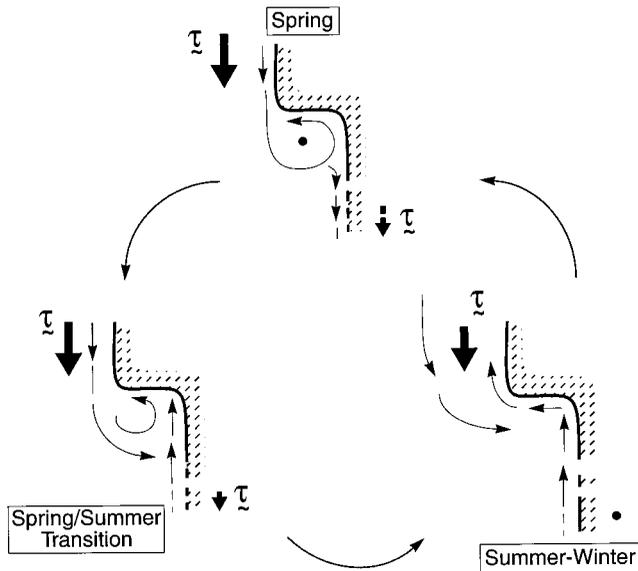
Figure 11. Schematics of the seasonal variations of the near-surface currents in the Santa Barbara Channel and the Southern California Bight, as a function of the wind distribution, inferred from the theories presented in the text. The seasonal cycle discussed in the text begins with Spring, then turns anticlockwise to spring/summer, summer-winter, then back to spring as directed by the arrows. Thick arrows denote wind stress, and thinner-lined arrows denote circulation.

the axis of the channel and weakens south and north near the coast (as well as to the east). Thus, along the northern portion of the channel, positive curl and along-coast gradient of the curl (i.e., larger cyclonic wind curl in the west than east) are established, and the sign is reversed along the southern portion. Since the timescale of response is short, of the order of 10 days, this windcurl distribution would produce, according to (13) in the LT limit, a westward (poleward) flow along the northern coast of the channel and an eastward flow along the southern coast. This mechanism is depicted schematically in Figure 12 and clearly depends on the existence of the coastal boundaries.

From spring into summer, over a timescale of 30–60 days, the large-scale effect of equatorward weakening of the wind curl over the SCB would have acted for a sufficiently long period that poleward flow begins to appear along the SCB coast. The timing for this would probably depend on the strength of the near-coast equatorward wind in the SCB (and farther south), which begins to weaken in summer into fall and winter [*Winant and Dorman*, 1997]. C. D. Winant (private communication, 1998) suggested that heating over the SCB in summer would also contribute to the strengthening of the poleward flow. Thus the poleward flow shown in Figure 11 for summer would consist of two complementing components: an alongshore wind curl gradient part in the PW limit according to (13) and a density-driven part due to heating over the SCB.

By end of summer and through fall and winter the alongshore wind curl gradient part in the PW limit would dominate forcing of the poleward flow, though it too weakens as the season progresses because of the more variable nature of the wind field, its mean being small compared to the amplitude of the variance ellipses [*Winant and Dorman*, 1997; *Harms and Winant*, 1998]. The more variable wind field suggests also that

the three forcing sources of the cyclone in the western SBC: localized wind curl, the along-coast gradients in wind curl in the LT limit (Figure 12), and eddy shedding [*Oey*, 1996], would weaken or be obliterated. As a result, flow in the channel is more likely to become more predominantly poleward.

Some questions remain. First, the springtime equatorward currents off PC and off the SCB are presumably remotely forced from farther south. There is little doubt that model incorporates this dynamic despite weak winds in the south [see *Oey*, 1996, Figures 16 and 17a]. Observational support (or refutation) of this is needed. Second, surface observations suggest that the wintertime poleward flow continues past PC into the central California coast [*Schwartzlose*, 1963; *Hickey*, 1979; C. D. Winant, private communication, 1998]. While this seems to agree with the above description of wintertime scenario, a detailed (re)analysis of observational data is needed to confirm that the poleward flow off central California is indeed caused by weakening of the wind curl south of PC; this would establish the dynamic link between poleward flow off SCB and the Davidson Current north of PC [*Hickey*, 1979]. Third, no attempt was made to describe short timescale current fluctuations, except for the three possible forcing mechanisms related to cyclone formation in the western SBC. This requires more in-depth model experiments, forced perhaps by more realistic wind conditions (from buoy stations). Fourth, hindcast experiments in progress give current energetics that are about half those observed; there were events that were not resolved by the coarse grid. The possibility of eddies that result via flow instability should be examined, perhaps with high-resolution grids <2 km [*Oey*, 1996, 1998]. Finally, the near-coast zone serves as a source of fluctuating currents that on the seasonal timescale may shift the axis of the California Current through westward propagating Rossby waves.
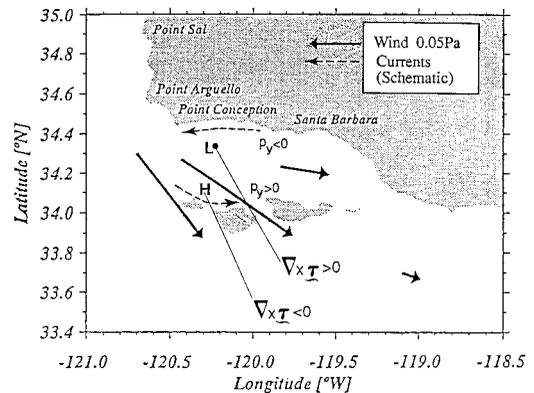
Figure 12. Spring wind stresses (solid vectors) at various buoy locations (from *Harms and Winant* [1998]) in the Santa Barbara Channel region, and schematics of the surface currents (dashed vectors) along the northern and southern coasts of the channel that illustrate the formation of a cyclonic recirculation in the western Santa Barbara Channel. Wind attains its maximum strength near the axis of the channel and weakens toward the coasts north and south. The result is cyclonic (anticyclonic) curl to the north (south), hence low (high) pressure as indicated by L (H). Thus a negative (positive) alongshore pressure gradient, p_y, in the north (south) drives westward (eastward) flow.

6. Conclusions

It is shown that when the wind distribution along a coast is anisotropic, such that its cross-shore scale is smaller than its alongshore scale, the forced Kelvin wave equation contains, in addition to the wind stress at the coast, a forcing term that is proportional to the time integral of the along-coast gradient of the wind curl. In practice this additional forcing is significant under two conditions: (1) when wind curl is intense (its cross-shore scale being of the order of the baroclinic Rossby radius) over a short period of 10 days or less and (2) when wind curl is less intense (and remains anisotropic) but persistent over seasonal timescales of O (months). Off the southern California coast and in the SBC these conditions are satisfied. The forcing then results in poleward flow near the surface.

Numerical experiments, from a simple reduced-gravity type with idealized forcing and coastline to a 3-D primitive equation model with realistic topography and observed wind stresses, were carried out to illustrate the flow dynamics. A comparison of the 3-D model results with the RG model shows that despite its simplicity the latter captures the main response of the former. It is shown that the equatorward weakening of the wind curl in the SBC is the dominant forcing that generates the near-coast near-surface poleward currents. Beta effect widens the current, provides a natural damping for the f plane–induced poleward flow, and produces a seasonal phase shift between the wind/wind curl, pressure field, and currents that leads to a better agreement with observations; it is otherwise not essential in producing the poleward flow near the coast.

References

Brink, K. H., and R. D. Muench, Circulation in the Point Conception-Santa Barbara Channel region, *J. Geophys. Res.*, *91*, 877–895, 1986.

Brink, K. H., D. W. Stuart, and J. C. Van Leer, Observations of the coastal upwelling region near 34°30′N off California: Spring 1981, *J. Phys. Oceanogr.*, *14*, 378–391, 1984.

Chen, C.-S., Model simulation on Santa Barbara Channel circulation, Ph.D. thesis, 83 pp., Mar. Sci. Res. Cent., State Univ. of N. Y. at Stoney Brook, 1998.

Gill, A. E., *Atmosphere-Ocean Dynamics*, 662 pp., Academic, San Diego, Calif., 1982.

Harms, S., Circulation induced by winds and pressure gradients in the Santa Barbara Channel, Ph.D. thesis, 138 pp., Univ. of Calif., San Diego, 1996.

Harms, S., and C. D. Winant, Characteristics patterns of the circulation in the Santa Barbara Channel, *J. Geophys. Res.*, *103*, 3041–3065, 1998.

Hickey, B. M., The California Current System: Hypotheses and facts, *Prog. Oceanogr.*, *8*, 191–279, 1979.

Hickey, B. M., Circulation over the Santa Monica-San Pedro basin and shelf, *Prog. Oceanogr.*, *30*, 37–115, 1992.

Huyer, A., P. M. Korso, S. J. Lentz, and R. C. Beardsley, Poleward flow in the California Current System, *Coastal Estuarine Sci.*, *34*, 142–156, 1989.

Gunn, J. T., P. Hamilton, H. J. Herring, K. L. Kantha, G. S. Lagerloef, G. L. Mellor, R. D. Muench, and G. R. Stegan, Santa Barbara Channel circulation model and field study, *rep. 92.1, 92.2*, Dynalysis of Princeton, Princeton, N. J., 1989.

Kolpack, R. J., *Biological and Oceanographical Survey in the Santa Barbara Channel Oil Spill 1969–1970*, vol. 2, 477 pp., Allan Hanock Found., Univ. of Southern Calif., Los Angeles, 1971.

Levitus, S., Climatological atlas of the world ocean, *NOAA Prof. Pap.*, *13*, 173, 1982.

McCreary, J. P., P. K. Kundu, and S.-Y. Chao, On the dynamics of the California current system, *J. Mar. Res.*, *45*, 1–32, 1987.

Oey, L.-Y., Flow around a coastal bend: A model of the Santa Barbara Channel eddy, *J. Geophys. Res.*, *101*, 16,667–16,682, 1996.

Oey, L.-Y., Eddy energetics in the Faroe-Shetland Channel: A model resolution study, *Cont. Shelf Res.*, *17*, 1929–1944, 1998.

Oey, L.-Y., and P. Chen, A nested-grid model simulation of the Norwegian coastal current, *J. Geophys. Res.*, *97*, 20,063–20,086, 1992.

Orlanski, I., A simple boundary condition for unbounded hyperbolic flows, *J. Comp. Phys.*, *21*, 251–269, 1976.

Reid, J. L., G. I. Roden, and J. G. Wyllie, Studies of the California current system, *Calif. Coop. Oceanic Fish. Invest. Prog. Rep. 7-1-56–1-1-58*, pp. 27–56, Mar. Resour. Comm., Calif. Dep. of Fish and Game, Sacramento, 1958.

Schwartzlose, R. A., Nearshore currents of the western United States and Baja California as measured by drift bottles, *Calif. Coop. Oceanic Fish. Invest. Prog. Rep. 7-1-60–6-3-62*, pp. 15–22, Mar. Resour. Comm., Calif. Dep. of Fish and Game, Sacramento, Calif., 1963.

Sverdrup, H. U., and R. H. Fleming, The waters off the coast of southern California, March to July 1967, *Scripps Inst. Oceanogr. Bull.*, *4*, 321–336, 1941.

Tsuchiya, M., Inshore circulation in the Southern California Bight, 1974–1977, *Deep Sea Res.*, *Part A*, *27*, 99–118, 1980.

Wang, D.-P., Effects of small-scale wind on coastal upwelling with application to Pt. Conception, *J. Geophys. Res.*, *102*, 15,555–15,566, 1997.

Winant, C. D., and C. E. Dorman, Seasonal patterns of surface wind stress and heat flux over the Southern California Bight, *J. Geophys. Res.*, *102*, 5641–5653, 1997.

Wyllie, J. G., Geostrophic flow of the California Current at the surface and at 200 m, *Calif. Coop. Oceanic Fish. Invest. Atlas* 4, xiii pp. and 288 charts, Calif. Dep. of Fish and Game, Sacramento, 1966.

L.-Y. Oey, Program in Atmospheric and Oceanic Sciences, Sayre Hall, Forrestal Campus, Princeton University, Princeton, NJ 08544. (lyo@splash.princeton.edu)